Bone 121 (2019) 243–254

Contents lists available at ScienceDirect

Bone

journal homepage: www.elsevier.com/locate/bone

Full Length Article

Absence of an osteopetrosis phenotype in *IKBKG* (NEMO) mutation-positive women: A case-control study

Morten Frost[a,b,c], Michaela Tencerova[c], Christina M. Andreasen[d,e], Thomas L. Andersen[e], Charlotte Ejersted[c], Dea Svaneby[f], Weimin Qui[c], Moustapha Kassem[c], Allahdad Zarei[i], William H. McAlister[g], Deborah J. Veis[h,i], Michael P. Whyte[h,i], Anja L. Frederiksen[a,j,*]

[a] Department of Clinical Research, Faculty of Health, University of Southern Denmark (SDU), Winsløwparken 19. 3, DK-5000 Odense C, Denmark
[b] Steno Diabetes Center Odense, Odense University Hospital (OUH), J.B. Winsløws Vej 4, DK-5000 Odense C, Denmark
[c] Department of Endocrinology, Molecular Endocrinology Unit, OUH, J.B. Winsløws Vej 4, DK-5000 Odense C, Denmark
[d] Orthopaedic Research Laboratory, Department of Orthopaedic Surgery & Traumatology, OUH, J.B. Winsløws Vej 15, DK-5000 Odense C, Denmark
[e] Department of Clinical Cell Biology, Vejle Hospital, Beridderbakken 4, DK-7100 Vejle, Denmark
[f] Department of Clinical Genetics, Vejle Hospital, Beridderbakken 4, DK-7100 Vejle, Denmark
[g] Department of Pediatric Radiology, Mallinckrodt Institute of Radiology, Washington University School of Medicine at St. Louis Children's Hospital, St. Louis, MO, USA
[h] Center for Metabolic Bone Disease and Molecular Research, Shriners Hospital for Children, St. Louis, MO, USA
[i] Division of Bone and Mineral Diseases, Department of Internal Medicine, Washington University School of Medicine at Barnes-Jewish Hospital, St. Louis, MO, USA
[j] Department of Clinical Genetics, Odense University Hospital, J.B. Winsløws Vej 4, DK-5000 Odense C, Denmark

ARTICLE INFO

Keywords:
NEMO
IKBKG
NF-κB
Osteopetrosis
X-chromosome inactivation
Incontinentia pigmenti

ABSTRACT

Background: NF-κB essential modulator (NEMO), encoded by *IKBKG*, is necessary for activation of the ubiquitous transcription factor nuclear factor kappa-light-chain-enhancer of activated B cells (NF-κB). Animal studies suggest NEMO is required for NF-κB mediated bone homeostasis, but this has not been thoroughly studied in humans. *IKBKG* loss-of-function mutation causes incontinentia pigmenti (IP), a rare X-linked disease featuring linear hypopigmentation, alopecia, hypodontia, and immunodeficiency. Single case reports describe osteopetrosis (OPT) in boys carrying hypomorphic *IKBKG* mutations.

Method: We studied the bone phenotype in women with IP with evaluation of radiographs of the spine and non-dominant arm and leg; lumbar spine and femoral neck aBMD using DXA; μ-CT and histomorphometry of transiliac crest biopsy specimens; bone turnover markers; and cellular phenotype in bone marrow skeletal (stromal) stem cells (BM-MSCs) in a cross-sectional, age-, sex-, and BMI-matched case-control study. X-chromosome inactivation was measured in blood leucocytes and BM-MSCs using a PCR method with methylation of *Hpa*II sites. NF-κB activity was quantitated in BM-MSCs using a luciferase NF-κB reporter assay.

Results: Seven Caucasian women with IP (age: 24–67 years and BMI: 20.0–35.2 kg/m^2) and *IKBKG* mutation (del exon 4–10 (n = 4); c.460C > T (n = 3)) were compared to matched controls. The *IKBKG* mutation carriers had extremely skewed X-inactivation (> 90:10%) in blood, but not in BM-MSCs. NF-κB activity was lower in BM-MSCs from *IKBKG* mutation carriers (n = 5) compared to controls (3094 ± 679 vs. 5422 ± 1038/μg protein,

Abbreviations: aBMD, areal bone mineral density; ACTB, beta-actin; ALP, alkaline phosphatase; AR, androgen receptor; ASBMR, American Society of Bone Mineral Research; AST, aspartate transaminase; AU, arbitrary units; BMD, bone mineral density; BMI, body mass index; BM-MSC, bone marrow mesenchymal stem cell; BS, bone surface; BV, bone volume; COL1A1, collagen of skin, type 1, alpha 1; CTX, cross-linked carboxyterminal telopeptide of type 1 collagen; DXA, dual-energy X-ray absorptiometry; ES, eroded surface; F.C., fold change; IP, incontinentia pigmenti; IQR, interquartile range; LH, linear hypopigmentation; LPS, lipopolysaccharides; MAR, mineral absorption rate; MLPA, multiplex ligation-dependent probe amplification; MS, mineralizing surface; NEMO, NF-κB essential modulator; NF-κB, nuclear factor kappa-light-chain-enhancer of activated B cells; Ob, osteoblast; Oc, osteoclast; OCN, osteocalcin; OPG, osteoprotegerin; OPT, osteopetrosis; OS, osteoid surface; Oc.S, osteoclast surface; PBMC, peripheral blood mononuclear cell; PCR, polymerase chain reaction; P1NP, pro-collagen type 1 amino terminal peptide; PTH, parathyroid hormone; QS, quiescent surface; RANKL, receptor activator of NF-κB ligand; RUNX2, Runt-related transcription factor 2; Rv.S, reversal surface; SD, standard deviation; SMI, structure model index; Tb.N, trabecular number; Tb.Sp, trabecular spacing; Tb.Th, trabecular thickness; TNFα, tumor necrosis factor alpha; TRAP, tartrate-resistant acid phosphatase; Th.N, trabecular number; TV, trabecular volume

* Corresponding author at: Dept. of Clinical Genetics, Odense University Hospital, J.B.Winsløws Vej 4, DK-5000 Odense C, Denmark.
E-mail addresses: morten.munk.frost.nielsen@rsyd.dk (M. Frost), mtencerova@health.sdu.dk (M. Tencerova), cmandreasen@health.sdu.dk (C.M. Andreasen), Thomas.Levin.Andersen@rsyd.dk (T.L. Andersen), Charlotte.Ejersted@rsyd.dk (C. Ejersted), Dea.Svaneby@rsyd.dk (D. Svaneby), mkassem@health.sdu.dk (M. Kassem), azarei@wustl.edu (A. Zarei), mcalisterw@mir.wustl.edu (W.H. McAlister), dveis@wustl.edu (D.J. Veis), mwhyte@shrinenet.org (M.P. Whyte), Anja.Frederiksen@rsyd.dk (A.L. Frederiksen).

https://doi.org/10.1016/j.bone.2019.01.014
Received 23 August 2018; Received in revised form 12 December 2018; Accepted 14 January 2019
Available online 16 January 2019

$p < 0.01$). However, no differences were identified on skeletal radiographics, aBMD, μ-architecture of the iliac crest, or bone turnover markers. The *IKBKG* mutation carriers had a 1.7–fold greater extent of eroded surfaces relative to osteoid surfaces ($p < 0.01$), and a 2.0–fold greater proportion of arrested reversal surface relative to active reversal surface ($p < 0.01$).

Conclusion: Unlike mutation-positive males, the *IKBKG* mutation-positive women did not manifest OPT.

1. Introduction

The nuclear factor kappa-light-chain-enhancer of activated B cells (NF-κB) essential modulator (NEMO) is the key activator of the ubiquitous transcription factor nuclear factor kappa-light-chain-enhancer of activated B cells (NF-κB) signalling pathway [1–3]. NF-κB signalling is in turn essential for regulation of bone growth and remodeling, initially demonstrated in mice deprived of both the NF-κB subunits p50 and p52 and impairment of osteoclast (Oc) differentiation leading to osteopetrosis (OPT) [4,5]. The receptor activator of NF-κB ligand (RANKL), expressed by osteoblasts (Obs), activates NF-κB in Oc precursor cells as well as Ocs, thereby promoting Oc differentiation and bone resorption [6]. Furthermore, NF-κB importantly regulates bone formation as NF-κB activation inhibits Ob differentiation [7–10]. Nevertheless, how NEMO balances NF-κB-mediated Ob and Oc responses is only partly understood.

Encoded by the X-chromosome located gene *IKBKG* [MIM: # 300248], global deficiency of NEMO is embryonically lethal in hemizygous male and homozygous female mice [11].

However, Swarnkar et al. [12] recently demonstrated arrested osteoclastogenesis and high bone mineral density in female mice carrying myeloid cell lineages with homozygous deletion of NEMO. Further, inhibition of NF-κB in NEMO dominant/negative transgenic female mice increased expression of the Ob marker gene Fos-related antigen-1 and bone mineral density (BMD), although the number of Obs was unchanged [13], suggesting that NEMO is critical for NF-κB-mediated bone homeostasis. In humans, pathogenic variants in *IKBKG* cause incontinentia pigmenti (IP [MIM: # 308300]), a rare X-linked disease clinically characterized by linear hypopigmentation, alopecia, hypodontia, abnormal tooth shape, dystrophic nails, ectodermal dysplasia, immunodeficiency, and neurocognitive disabilities [14]. The pleomorphic features of IP are partly explained by genotype-phenotype associations and X-chromosome inactivation [14,15]. Deletion of *IKBKG* exon 4–10, the most prevalent "loss-of-function" mutation (~65%) [16,17], is embryonically lethal in human male fetuses, whereas hypomorphic sequence variants may permit survival of boys and generally cause milder phenotypes in girls and women [18]. Nevertheless, only a few case reports describe a skeletal phenotype in young *IKBKG* mutation male carriers [19–24].

Generalized osteosclerosis with increased BMD can occur in skeletal dysplasias, and infectious or neoplastic diseases [25]. In osteopetrosis (OPT), increased BMD results from impaired Oc activity, sometimes due to decreased numbers of these cells. An OPT bone phenotype was described in 2001 by Döffinger et al. [19] in two brothers with an *IKBKG* missense mutation and generalized osteosclerosis, and that same year bone fractures were reported in a two-year-old boy with a nonsense *IKBKG* mutation [20]. Similarly, in 2010, a boy age 18 months carrying a minor deletion in *IKBKG* [21] reportedly had radiographic findings compatible with OPT. Also, radiographic "bone-within-bone" appearance in iliac wings characteristic of OPT has been described in two boys with either an *IKBKG* missense or a stop mutation [22,23]. Iliac crest biopsy of the latter boy showed dense, irregular trabeculae with apparently normal numbers and morphology of Ocs, suggesting impaired Oc activity rather than decreased numbers Ocs accounted for the increased bone density. The trabeculae were reported to have a central core of cartilage as proof of Oc failure and therefore OPT [23]. In contrast, no radiographic sign of OPT was observed in a boy with an *IKBKG* splice site variant despite the IP phenotype [24].

To our knowledge, these reports are the available descriptions of the skeletal findings in *IKBKG* mutation-positive people. Although women with *IKBKG* mutations develop clinical evidence of IP, skeletal abnormalities have been reported only in young *IKBKG* mutation carrier males. Therefore, it remains to be investigated if women with an *IKBKG* mutation develop OPT. In addition, studies of humans with certain rare monogenetic disorders provide a unique research strategy to understand skeletal signalling pathways in bone metabolism and more common disorders including osteoporosis. Herein, we explored if Danish women with features of IP carrying an *IKBKG* mutation manifest an OPT phenotype as previously described in boys.

2. Methods

2.1. Subjects

This was a prospective, cross-sectional, case-control study. Participants were women > 18 years of age known to carry a pathogenic *IKBKG* variant (i.e. *IKBKG* mutation carriers) and a healthy control group matched for sex, age, and body mass index (BMI). Exclusion criteria included renal (creatinine > 90 μmol/L) or liver (aspartate transaminase > 3 times the upper limit) dysfunction, medical treatment that could influence bone metabolism (oral corticosteroid within the last 12 weeks and treatment with anti-osteoporosis medication, sex steroids, anticonvulsants), metabolic bone diseases, pregnancy, excessive alcohol consumption (> 14 units/week), anticoagulant treatment, pre-existing coagulopathy, or allergy to lidocaine, morphine, or diazepam.

The study was approved by the Ethic Committee, Region of Southern Denmark (S-20150124) and the Danish Civil Data Registry (Nr. 16/983). Signed informed consent was obtained from all study subjects.

Twenty women diagnosed with IP at the Department of Clinical Genetics, Odense University Odense, Vejle Hospital, Aarhus University Hospital, and Rigshospitalet, Copenhagen, in Denmark were invited by letter to participate in the study. Seven responded positively. All seven underwent systematic interview about their medical history including bone fractures, selective radiographic skeletal imaging, dual-energy X-ray absorptiometry (DXA), and fasting blood sampling. One *IKBKG* mutation carrier declined sampling of bone marrow and bone tissue. Subsequently, six *IKBKG* mutation carrier and six matched controls underwent transiliac crest bone biopsy following tetracycline "labelling" given orally, and separately bone marrow aspiration from the posterior iliac spine. The two procedures were unsuccessful in one *IKBKG* mutation carrier.

Controls were recruited using public advertisements. The period of recruitment was February 1st to August 1st 2016.

2.2. Genetic analyses

Multiplex ligation-dependent probe amplification (MLPA) analysis was used to detect the recognizable deletion of exons 4–10 within *IKBKG*. If the test was negative, the DNA was analysed by Sanger sequencing. X-chromosome inactivation was measured by a standard polymerase chain reaction (PCR) method that involved methylation of *Hpa*II sites located next to the polymorphic CAG-repeat in the androgen receptor gene (*AR*) [26].

2.3. Laboratory evaluations

To exclude common disorders that could affect bone metabolism, fasting blood samples were analysed for total Ca^{2+}, ionized Ca^{2+}, parathyroid hormone (PTH), 25-(OH)-vitamin D, p-aspartate transaminase, p-lactate dehydrogenase, p-thyroid stimulating hormone, p-IgA, p-IgG, and p-IgM levels in all participants (n = 14). Furthermore, bone turnover markers were measured in peripheral blood. In fasting serum, pro-collagen type 1 amino terminal peptide (P1NP), cross-linked carboxyterminal telopeptide of type 1 collagen (CTX-I), and osteocalcin (OCN) were quantitated using IDS-iSYS (Immunodiagnostic Systems Tyne and Wear, UK), and sclerostin was quantified with the Human Sclerostin HS EIA Kit according to the manufacturer's protocol (TECOmedical AG©2016, Sissach, Switzerland). In single analyses, osteoprotegerin (OPG) was measured using a Sandwich ELISA horseradish peroxidase (HRP)/tetramethyl benzene (TMB) method, whereas RANKL was measured as free soluble RANKL, both according to Biomedica Immunoassays (Biomedica Immunoassays, Vienna, Austria).

2.4. Radiographic studies

Antero-posterior projection radiographs of the non-dominant humerus, thoracolumbar spine, pelvis, and proximal femur as well as lateral projection radiographs of the thoracolumbar spine were evaluated by radiologist William H. McAlister, MD, for evidence of any generalized skeletal disease in all participants (n = 14). All images were evaluated “blindly” and in random order before comparing the *IKBKG* mutation carriers to the control group.

2.5. DXA scans

Areal bone mineral density (aBMD) was measured using DXA (Hologic Discovery, Waltham, Massachusetts, USA) in an anterior-posterior projection at the lumbar spine (L1–L4), total hip, and femoral neck in all participants (n = 14). The Z-scores were calculated using the reference ranges provided by the manufacturer and by the Third National Health and Nutrition Examination Survey reference [27]. Evaluation of the DXA scan for subsequent calculations was observer blinded.

2.6. Bone biopsy

Transiliac crest bone biopsies were collected after each study subject (*IKBKG* mutation carriers n = 5, controls n = 5) underwent double labelling with tetracycline administrated orally. Prior to the bone biopsy, the *IKBKG* mutation carriers and controls ingested tetracycline hydrochloride 250 mg three times daily on days 1–3 and 13–15. On day 20, a 7 mm diameter core was obtained across the iliac crest [28]. The specimens were separately fixed and stored in 70% ethanol/30% water at 4 °C until dehydrated and embedded non-decalcified in methyl-methacrylate. Subsequently, 7.5-μm–thick sections were cut and stained for detailed histomorphometric analyses.

2.7. Bone marrow aspiration

Bone marrow (10 ml) was obtained in *IKBKG* mutation carriers (n = 5) and matched controls (n = 5) by aspiration from the iliac crest and mixed with 10 ml of heparin (100 U/ml) and subsequently used for isolation of BM-MSCs. Low-density mononuclear cells were isolated by centrifugation with a density gradient medium (Lymphoprep™, STEMCELL technologies, Cambridge, UK) (density = 1.077 ± 0.001 g/cm^2), and then selected using plastic adherence. Cells were then cultured at 1×10^5 cells/cm^2 (1×10^6 cells per chamber slide) in Minimal Essential Media (MEM) containing 10% fetal bovine serum (FBS), incubated at 5% CO_2 at 37 °C, and then cultured by changing the medium weekly along with passage when 70% confluent. The cultured cells were used for subsequent molecular analysis of expression profiles of genes specifically involved in NF-κB signalling as well as measurement of NF-κB activity.

2.8. Micro-CT scanning

The whole iliac crest biopsy specimen (n = 10) was scanned using a μCT scanner (μCT 50, Scanco Medical AG, Brüttisellen, Switzerland) with an isotropic voxel size of 6 μm (X-ray tube: 155 μA, 90 kVp, integration time 1500 ms) to quantify the 3D microarchitectural properties of the cancellous bone [29]. All specimens were scanned in the same orientation. The 3D-image data sets, filtered with a Gaussian filter (sigma = 0.8, support = 1) and segmented with an optimal threshold of 180 consisted of approximately 600 consecutive 16-bit gray scale images. These images were used to quantify (after segmentation with a fixed optimal threshold) bone volume fraction (BV/TV, %), trabecular thickness (Tb.Th, μm), trabecular spacing (Tb.Sp, μm), trabecular number (Tb.N, mm^{-1}), structure model index (SMI), and connectivity density (mm^{-3}) [30].

2.9. Histomorphometry

Consecutive sections were cut from the whole biopsy from each *IKBKG* mutation positive carrier (n = 5) or control subject (n = 5). The sections were analysed either unstained or as pairs stained with: i) Goldner's Trichrome, or ii) tartrate-resistant acid phosphatase (TRAP), a histochemical activity marker of Ocs [31]. Prior to the analysis the sections from the ten biopsies were blinded.

2.9.1. Static histomorphometry

Micrographs of the stained sections were printed as maps, and the extent of eroded surface (ES), osteoid surface (OS), reversal surface (Rv.S), osteoclast surface (Oc.S), and quiescent surface (QS) was marked on the bone surface (BS) within these maps. The reversal surface was subdivided into either “active” or “arrested”. In contrast to arrested reversal surfaces, active reversal surfaces were flanked by Ocs and/or OS [32]. A second blinded observer validated the markings of the respective surfaces. The extent of the surfaces was estimated by counting the number of intercepts between a cycloid grid and the particular surfaces (Fig. 2A). More precisely, the number of intercepts with a particular surface was divided with total number of intercepts to calculate the extent of the following surfaces; osteoid, eroded, quiescent, osteoclast as well as reversal surfaces (including “active” and “arrested”) per bone surface. On average, 647 (range 356–941) intercepts were counted for each *IKBKG* mutation-positive case, and 675 (range 240–1229) for each control.

2.9.2. Dynamic histomorphometry

Unstained sections were scanned with a NanoZoomer HT (Hamatasu, Bridgewater, NJ, USA) system (P30 NS057105) at 0.46 μm/pixel, 20× magnification on brightfield and fluorescence (FITC and TRITC) modes. The scans were read using a semi-automatic image analyser system (Bioquant, Nashville, TN, USA). Analysis was performed in the cancellous bone in a region of interest 200 μm from the cortico-medullary junction(s), on average encompassing 220 μm^2 per specimen. Surfaces bearing a single or double label were read and the thicknesses between the two labels were measured. Mineral apposition rate (MAR) and mineralizing bone surface (MS/BS) were calculated according to ASBMR guidelines [33] (Fig. 2I).

2.10. Cell-studies

2.10.1. NF-κB reporter assay

BM-MSCs from the *IKBKG* mutation carriers (n = 5) and the healthy controls (n = 5) and were isolated and seeded at a density of 12,000 cells/cm^2 in a 96-well plate, and subsequently infected with a pLenti-NFκB-Luc reporter (Qiagen, Hilden, Germany) (MOI = 4–6). The following day, the cells were treated with or without lipopolysaccharides (LPS) (1 μg/ml) for 3 h. The luciferase assay was performed using a luciferase assay system (Promega, Madison, WI, USA) and normalized against the protein concentration measured using a Pierce™ Coomassie (Bradford) Protein Assay Kit (ThermoFisher Scientific, Waltham, MA, USA).

2.10.2. Quantification of osteoclasts

Human Oc precursors were prepared from peripheral blood (50 ml) using the protocol of Boissy et al. [34]. The peripheral blood mononuclear cells (PBMCs) were separated by centrifugation using a Ficoll-Paque PLUS (Amersham Biosciences, Hillerød, Denmark). Then, monocytes were isolated by magnetic cell sorting according to the manufacturer's instructions using biotinylated anti-human CD14 goat antibody (R&D Systems, Abingdon, UK). Sorted cells were pre-treated with M-CSF for 3 days, trypsinized and counted, and subsequently plated as 20,000 cells/well in a 96 well plate (6000/cm^2). Cells were differentiated with 25 ng/ml RANKL and 25 ng/ml M-CSF (at seeding), and the media changed every 2nd day. Mature Ocs; defined as multinuclei cells with 3 or more nuclei, were quantified after D10 of differentiation by staining for TRAP.

2.10.3. Osteoblast differentiation of BM-MSC

The cells were plated at a density of 20,000 cells/cm^2 in alpha MEM medium (Gibco) containing 10% FBS, 100 U/ml penicillin (Gibco), and 100 μg/ml streptomycin (Gibco). Osteoblast induction media comprised of base medium supplemented with 10 mM B-glycerophosphate (Sigma-Aldrich), 10 nM dexamethasone (Sigma-Aldrich), 50 μg/ml Vitamin C (Sigma-Aldrich) and 50 μg/ml Vitamin D (Sigma-Aldrich) replaced media one day after the seeding. The medium was changed every other day for 10 days.

2.10.4. Alkaline phosphatase (ALP) activity assay

Cells were incubated with naphthol AS-TR phosphate solution containing Fast Red TR (Sigma-Aldrich) as described previously [35]. ALP activity was measured using p-nitrophenyl phosphate (Fluka Chemie) as substrate.

2.10.5. Gene expression analysis

BM-MSCs and Ocs from *IKBKG* mutation-positive carriers and healthy controls (n = 5 per group) were seeded in 12-well plates and then treated with or without LPS (1 μg/ml) for 3 h. Ob differentiated BM-MSC samples were used for RNA isolation. Total RNA was isolated using the Trizol method (ThermoFisher Scientific, Waltham, MA, USA), and 1 μg total RNAs was reverse transcribed by iScript™ cDNA synthesis kit (Bio-Rad, Hercules, CA, USA). Real-time RT-PCR of the NF-κB responsive gene tumor necrosis factor alpha (TNFα) and of the NF-κB subunit p65 was performed using fast SYBR Green master mix (Applied Biosystem, Foster City, CA, USA) on a StepOnePlus™ system according to the manufacturer's protocol. Gene expression was normalized to a housekeeping gene *ACTB* (beta (β)-actin). The observer was blinded to the subject identity. The primer sequences were: *ACTB*, beta (β)-actin: forward (5′-3′) ATTGGCAATGAGCGGTTCCG; reverse (3′-5′) AGGGCAGTGATCTCCTTCTG; p65 (Rela): forward (5′-3′) GAACCAGGGCATACCTGTGG; reverse (3′-5′) TAGCCTCAGGGTACTCCATCA; TNFα: forward (5′-3′) ATGAGCACTGAAAGCATGATCC; reverse (3′-5′) GAGGGCTGATTAGAGAGAGGTC); *ALPL* forward (5′-3′): ACGTGGCTAAGAATGTCATC, reverse (3′-5′): CTGGTAGGCGATGTCCTTA; RUNX2: forward (5′-3′): TGGTTACTGTCATGGCGGGTA, reverse (3′-5′): TCTCAGATCGTTGAACCTTGCTA and BGLAP: forward (5′-3′): CATGAGAGCCCTCACA, reverse (3′-5′): AGAGCGACACCCTAGAC.

2.11. Statistics

Data distribution was examined using the Shapiro-Wilks normality test, and presented as mean ± SD or median [IQR] according to their distribution. Differences between matched groups were assessed with a paired *t*-test for parametric data and Wilcoxon's matched-pair signed-rank test for non-parametric data. Clustered logistic regression adjusted for age was used for calculation of odds ratios. A p-value < 0.05 was considered statistically significant. An unpaired *t*-test was used for the molecular studies. All statistical analyses were performed using the Stata Statistical Software 12.0 (StataCorp LP, College Station, TX, USA).

3. Results

3.1. Characterization of the patient cohort: genotype and clinical findings

Seven *IKBKG* mutation-positive Caucasian women and seven controls matched for age and BMI were studied (Table 1). All *IKBKG* mutation carriers manifested one or more findings associated with *IKBKG* mutations and IP (Table 2). However, similar to the controls, none reported low-energy fractures. Four *IKBKG* mutation positive carriers harboured an *IKBKG*exon4_10del. The remaining three mutation carriers, including the mother, carrier no. 5, and her daughter, carrier no. 6, harboured a missense mutation, *IKBKG*, c.460C > T, p.Q154X (Table 2).

3.2. IKBKG mutation carriers have extremely skewed X-inactivation in blood leucocyte and normal distribution of X-inactivation in BM-MSCs

Six of the 7 *IKBKG* mutation carriers had extremely skewed X-inactivation > 90:10% in their blood leucocytes, whereas only 1 of 5

Table 1
Demographics of *IKBKG* mut^+ carriers and controls.

	IKBKG mut^+ carriers	Controls	p-Value
Number	7	7	–
Age (years)	34 [25–59]	42 [26–46]	p = 0.85
Weight (kg)	66.1 [55.9–73.2]	66.2 [61.2–71.0]	p = 0.65
Height (cm)	162.0 [161.6–168.9]	166.8 [162.7–171.7]	p = 0.11
BMI	23.5 [20.3–27.8]	22.8 [22.4–27.8]	p = 0.89

Wilcoxon's matched-pair signed-rank. Median [IQR].

Table 2
Demographics and clinical characteristics of the *IKBKG* mutation carriers.

IKBKG – mut$^+$ carrier, #	Age (years)	Height (cm)	Weight (kg)	BMI (kg/m^2)	Gentype *IKBKG*	X-inactivation, blood (%)	X-inactivation, BM-MSC (%)	Alopecia	Hypodontia/ abnormal shape	Dystrophic nails	Skin	Other features
1	34	172	104	35.2	Del exon4–10	97:3	67:33	+	−/+	+	B/LH	Retinal changes
2	59	162	61	23.5	Del exon4–10	83:17	65:35	+	+/−	+	B/LH	–
3	34	162	67	25.9	Del exon4–10	93:7	N.A.	+	+/−	+	B/LH	–
4	67	169	66	23.4	c.460C > T	97:3	94:6	−	−/−	−	N.A.	–
5	47	162	73	27.8	c.460C > T	94:6	71:29	−	+/−	+	B/LH	–
6	25	166	56	20.0	c.460C > T	100:0	68:32	−	+/+	−	B/LH	–
7	24	160	52	20.3	Del exon4–10	90:10	N.A.	+	+/+	+	LH	–

Data are presented as median [IQR] Subject nr 6. is daughter of no. 5. Skin blistering (B). Linea hypopigmentation (LH). N.A.: information not available. (?): symptoms present. (−): symptoms absent.

Table 3
Biochemistry and bone turnover markers in *IKBKG* mutation carriers versus controls.

	IKBKG mut$^+$ carrier (n = 7)	Controls (n = 7)	p-value
p-Ca^{2+} (mmol/L)	1.25 ± 0.04	1.27 ± 0.03	p = 0.81
p-AST (U/L)	29 [21–37]	23 [18–23]	p = 0.27
p-LD (U/L)	196 ± 22	182 ± 50	p = 0.27
p-TSH (10E − 3 IU/L)	1.73 ± 0.72	1.81 ± 0.87	p = 0.57
p-IgA (g/L)	1.65 ± 0.63	1.98 ± 0.44	p = 0.86
p-IgG (g/L)	11.2 [10.5–12.3]	11.2 [10.1–13.6]	p = 0.75
p-IgM (g/L)	1.64 ± 0.89	1.34 ± 0.58	p = 0.23
25-(OH) vit. D (nmol/L)	53 ± 27	67 ± 21	p = 0.85
p-PTH (pmol/L)	2.97 [1.58–4.23]	2.21 [1.71–5.98]	p = 0.95
p-CTX (μg/L)	0.29 [0.20–0.35]	0.48 [0.21–0.61]	p = 0.34
p-PINP (μg/L)	54.5 [43.3–69.7]	76.3 [53.7–81.8]	p = 0.40
p-OC (ng/mL)	18.1 [14.9–41.1]	24.4 [20.1–34.6]	p = 0.65
p-Sclerostin (pmol/L)	0.64 [0.42–0.77]	0.45 [0.41–0.53]	p = 0.14
p-RANKL (pmol/L)	0.15 [0.11–0.20]	0.20 [0.09–0.23]	p = 0.56
p-OPG (pmol/L)	4.52 [4.39–4.80]	5.42 [3.59–5.67]	p = 0.57

Data are presented as mean ± SD or median [IQR].

IKBKG mutation carriers (carrier no. 4) had extremely skewed X-inactivation in her BM-MSCs. Determination of parental origin of the inactive X chromosome was possible for only one individual (carrier no. 6), which showed the maternal (and thus *IKBKG* mutated) X chromosome was silenced (Table 2).

3.3. IKBKG mutation carriers have normal biochemical parameters

No differences in biochemical parameters of bone metabolism were noted in the *IKBKG* mutation carriers compared to the controls, including p-Ca^{2+}, p-25-(OH) vitamin D, PTH, CTX, P1NP, OCN, sclerostin, RANKL, or OPG (Table 3).

3.4. There are no differences between IKBKG mutation carriers and controls in skeletal findings on radiographic evaluation or micro-CT-scanning

For investigation of the macroscopic bone phenotype, the question asked of the blinded radiologist had been: “Is there evidence of a generalized systemic skeletal disorder with low or high bone density or modeling abnormalities?” No such differences were noted in the radiographs of the *IKBKG* mutation carriers compared to the controls. Their skeletons were found to be normally shaped without signs of osteosclerosis (Fig. 1A and B). Furthermore, no significant differences were noted in aBMD, bone mineral content, or bone area, or femur axis length comparing the *IKBKG* mutation carriers to the controls (Table 4).

On μ-CT-scanning, borderline significant lower trabecular thickness was noted in the *IKBKG* mutation carriers versus controls (p = 0.066), and no significant differences were noted for the microstructural parameters (Fig. 1C and D, Table 5).

3.5. IKBKG mutation carriers have higher proportion of eroded surfaces relative to osteoid surfaces, and higher arrested versus active reversal surfaces

Static histomorphometry of specific bone surfaces, by counting the number of intercepts between a cycloid grid and the particular surfaces (Fig. 2A), showed no significant differences between *IKBKG* mutation carriers and controls (Table 6). However, the *IKBKG* mutation carriers had a 1.7-fold higher extent of eroded surfaces relative to osteoid surfaces ($p < 0.01$) (Fig. 2B, E). Because approximately 90% of the eroded surfaces were reversal surfaces, they were further characterized. A proportion of them were arrested reversal surfaces with no neighboring OS or Oc (Fig. 2D). Compared to the controls, *IKBKG* mutation carriers had a 2.0–fold higher proportion of arrested versus active reversal surfaces ($p < 0.01$) (Fig. 2C, F). Interestingly, in both the *IKBKG* mutation carriers and the controls, the arrested reversal surfaces versus active reversal surfaces had a 5.2–fold higher proportion of superficial resorption depths (1–2 broken double-lamellae) relative to deep resorption depths (> 2 broken double-lamellae) (Fig. 2G).

The dynamic histomorphometric analyses revealed that the extent of mineralizing surfaces; i.e. mineral surface relative to bone surfaces (MS/BS), was lower in the *IKBKG* mutation carriers than in the controls (Fig. 2H) whereas the mineral apposition rate (MAR) was similar in both groups (Fig. 2I). There were no signs of retention of cartilage within the trabecular bone of either study group.

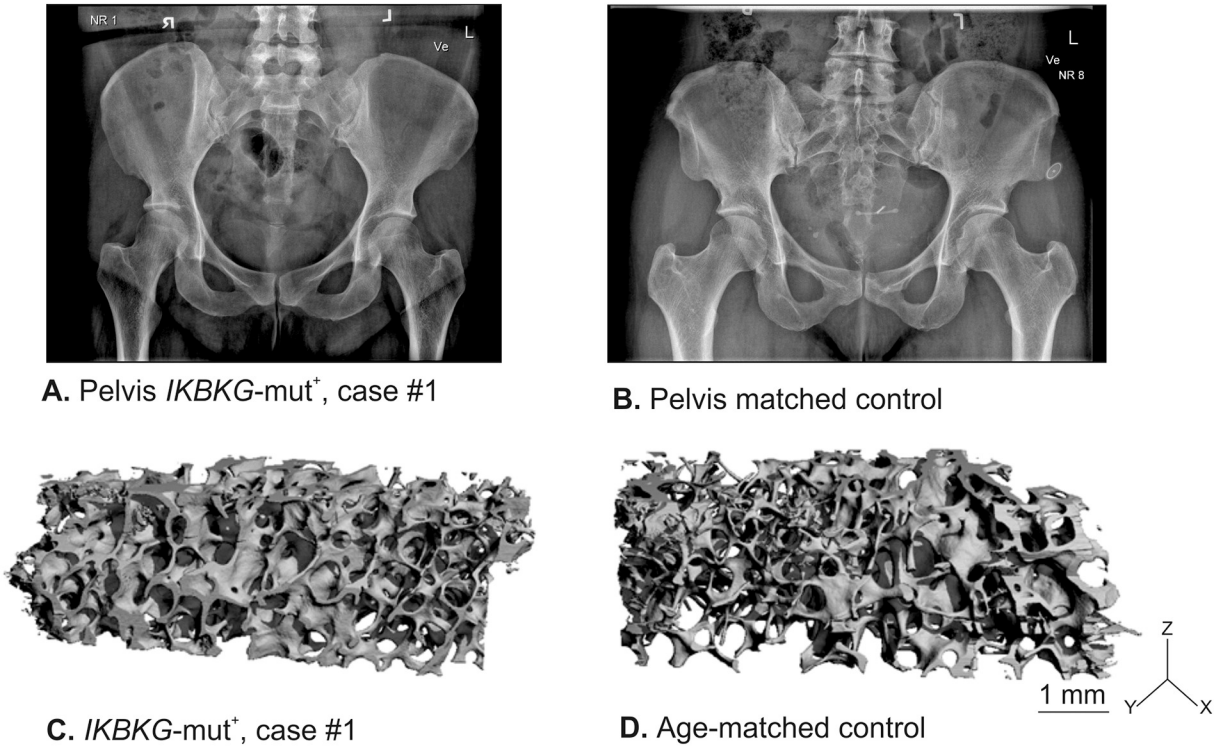

Fig. 1. Radiographic comparison of a *IKBKG* mutation-positive woman with IP versus control.
(A) Anteroposterior pelvis from *IKBKG* mutation-positive carrier # 1.
(B) Anteroposterior pelvis from matched control.
There is no suggestion of an osteopetrosis phenotype in the *IKBKG*-mutation positive carrier.
Micro-CT based bone structure in mutation-positive women versus controls. 3D reconstruction of consecutive micro-CT images of trabecular bone in iliac crest biopsies from *IKBKG* mutation-positive carrier (C) and control (D).
There is no suggestion of altered structure of ilial cancellous bone in the *IKBKG* mutation carrier.

Table 4
Bone mineral areal density and mineral content by DXA in *IKBKG* mutation carriers versus controls.

Parameters	*IKBKG* mut$^+$ carrier (n = 7)	Controls (n = 7)	p-Value
Lumbar spine, area (cm^2)	51.9 ± 16.8	62.1 ± 9.9	p = 0.19
Lumbar spine, BMC (g)	59.7 [51.9–65.2]	71.6 [46.0–81.1]	p = 0.40
Lumbar spine, BMD (g/cm^2)	1.05 [0.90–1.10]	1.04 [0.83–1.20]	p = 0.85
Lumbar spine (Z-score)	0.5 [0.0–0.7]	0.6 [(−1.9)–1.4]	p = 0.61
Femur neck area (cm^2)	4.82 [4.60–5.21]	5.29 [4.61–5.64]	p = 0.48
Femur neck, BMC (g)	3.49 [2.92–4.06]	4.29 [3.07–4.99]	p = 0.22
Femur neck, BMD (Z-score)	0.72 [0.63–0.83]	0.80 [0.65–0.97]	p = 0.41
Total hip areal (mm^2)	32.7 [30.3–34.8]	34.3 [31.0–41.2]	p = 0.34
Total hip, BMC (g)	28.7 [25.5–29.9]	31.4 [23.1–37.6]	p = 0.48
Total hip, BMD (g/cm^2)	0.86 [0.78–1.02]	0.85 [0.75–1.06]	p = 0.95
Total hip (Z-score)	−0.3 [−0.6–(0.69)]	−0.4 [(−1.6)–1.0]	p = 0.90
Hip axis length (cm)	107.3 [100.3–110.1]	109.6 [103.0–111.8]	p = 0.57

BMD = bone mineral density, BMC = bone mineral content. Data are presented as mean ± SD (normal distribution) or median [IQR].

3.6. No differences in number of TRAP positive osteoclasts or gene expression of mRNA p65 or TNFα

To further elucidate the molecular phenotype of Ocs in *IKBKG* mutation carriers, we performed cellular analysis of isolated cells. Quantifying Oc differentiation from PBMCs did not show a significant difference in the number of TRAP positive Ocs between *IKBKG* mutation carriers and controls (Fig. 3A–B) confirming the data showing extremely skewed X-inactivation in blood leukocytes, that circulating Oc precursors were not affected by *IKBKG* mutation. In addition, LPS-stimulated expression of mRNA p65 (RelA) and TNFα did not show any differences between the groups (Fig. 3C and D).

3.7. NF-κB activity is decreased in BM-MSCs in IKBKG mutation carriers

To investigate the degree to which the NF-κB pathway was inactivated in the BM-MSCs, the NF-κB activity response to LPS stimulation was evaluated by the NF-κB reporter assay. This procedure revealed lower NF-κB activity in the *IKBKG* mutation carriers compared to the controls (Fig. 4A). NF-κB activity was lower in the *IKBKG* mutation carriers with *IKBKG*exon4_10del (2922 ± 93/μg protein) and in the carriers with *IKBKG* c.460C > T (3209 ± 412/μg protein, $p < 0.01$) (Fig. 4B).

Further, we investigated expression of NF-κB pathway-related genes such as p65/(RelA) NF-κB subunit and TNFα, NF-κB responsive gene. In their BM-MSCs, the *IKBKG* mutation carriers had lower p65/(RelA) and

Table 5
Structural properties (mean ± SD) of ilium cancellous bone in *IKBKG* mutation carriers and their controls listed as age-matched pairs.

	Biopsy #	Volume fraction (%)	Trabecular thickness (μm)	Trabecular spacing (μm)	Trabecular number (#)	Connectivity density (mm^{-3})
IKBKG mut^+ carriers (n = 5)	1	18.7	119.4	636.8	1.5	7.90
	2	11.1	138.3	833.1	1.1	4.50
	4	8.4	108.3	796.8	1.2	5.87
	5	14.0	140.5	743.8	1.3	5.54
	6	16.0	136.0	704.5	1.3	6.01
	Mean ± SD	13.64 ± 4.03	128.5 ± 14.03	743.0 ± 77.09	1.29 ± 0.14	5.96 ± 1.23
Controls (n = 5)	8	15.3	138.8	762.7	1.2	5.20
	16	9.9	157.5	754.7	1.3	5.78
	11	17.1	145.7	807.5	1.2	4.09
	12	14.6	132.1	726.2	1.3	6.76
	14	20.3	172.3	876.7	1.1	4.23
	Mean ± SD	15.45 ± 3.81	149.28 ± 15.93	785.6 ± 58.71	1.21 ± 0.08	5.21 ± 1.11
IKBKG mut^+ carriers vs. controls	p-Value	0.451	0.066	0.411	0.362	0.419

TNFα mRNA levels in response to LPS stimulation, respectively (Fig. 4C and D).

In addition, we tested whether inactivation of the NF-κB pathway in BM-MSCs could affect osteoblast (Ob) differentiation. While there were no differences in ALP activity between groups (Fig. 4E), or in gene expression of the Ob markers RUNX2 and ALPL, the mRNA levels of *BGLAP* were significantly higher in *IKBKG* mutations carriers compared to controls (Fig. 4F).

4. Discussion

Our review of the publications describing an OPT bone phenotype in boys harbouring *IKBKG* mutations [19–24] revealed radiographic images of the skeleton consistent with OPT in three reports [20,22,23]. In contrast, our investigation that included a radiographic survey and DXA, did not identify any evidence of osteosclerosis in *IKBKG* mutation carrier women. To our knowledge, bone histomorphometry has been reported only in one boy with NEMO deficiency [23]. Here, in 2002, the investigators described normal Oc numbers and morphology as well as large and dense trabeculae with a central core of cartilage. Our micrographs showed no difference in the proportion of Oc surface in women with IP (data not shown), indicating that impaired NEMO activity does not decrease the proportion of the Oc surface. The trabecular thickness did tend to be lower in the *IKBKG* mutation carriers, but did not reach statistical significance. This is in contrast to the frequent finding of *increased* trabecular thickness in mouse models and children with OPT [36–38]. However, studies of a larger cohort would be necessary to know if NEMO deficiency reduces trabecular thickness.

Bone remodeling constitutes the highly coordinated and balanced process of bone resorption and formation linked by the intermediate reversal phase [39]. Uncoupling of the reversal phase in postmenopausal and glucocorticoid-induced osteoporosis leads to decreased osteoid surface and increased eroded surface [32,40]. Notably, we observed in *IKBKG* mutation carriers a decrease in the extent of mineralizing bone surface and an increase in the ratio between eroded and osteoid (formative) surfaces. In aging and osteoporotic patients, a similar change in the extent of formative surfaces and the ratio of eroded surfaces has been linked with a delayed initiation of bone formation due to prolongation of the reversal-resorption phase [31,32]. In studies of cancellous bone, cumulative eroded surfaces were shown to have a higher proportion of arrested versus active reversal surfaces in osteoporotic patients [32,41], as observed for the *IKBKG* mutation carriers in our study. In contrast, rabbits treated with odanacatib, an inhibitor of Oc secreted cathepsin K, presented a shorter reversal phase and increased initiation of bone formation [42]. To some extent, these cathepsin K-inhibitor treated rabbits reflect what we had expected to observe, if the *IKBKG* mutation carriers were osteopetrotic. Initiation of bone formation requires a critical density of Ob progenitors, i.e. reversal cells are recruited to the eroded surfaces during the reversal-resorption phase [43]. Accordingly, one may argue that the length of the reversal-resorption phase is dependent on the rate of Ob progenitor recruitment, and that insufficient Ob recruitment and differentiation may prolong the reversal-resorption phase and delay the initiation of bone formation. Hence, the prolonged reversal phase and reduced extent of bone formation in *IKBKG* mutation carriers could reflect insufficient recruitment and differentiation of Ob progenitors. This hypothesis is supported by accumulation of arrested reversal surfaces in *IKBKG* mutation carriers because these surfaces have a much lower density of osteoprogenitor cells and active reversal surfaces [41,42].

In addition to stimulating Oc differentiation and activity, classic NF-κB signalling also inhibits Ob differentiation [7–10]. Therefore, decreased NEMO activity would be expected to enhance Ob differentiation, potentially increasing bone formation, and possibly contributing to the osteosclerosis reported in NEMO-deficient boys [19–21,23]. We note that gene expression of the Ob marker osteocalcin was higher in *IKBKG* mutation BM-MSCs of the *IKBKG* mutation carriers, yet we did not find evidence in these mutation-positive women for increased bone formation in either their circulating bone turnover or their bone histomorphometry. This suggests that deactivating *IKBKG* mutations do not significantly up-regulate bone formation.

Our finding of lower NF-κB activity in BM-MSCs from the *IKBKG* mutation carriers is consistent with diminished NEMO activation of NF-κB. Lower gene expression of p65 and TNFα in these cells was concordant with the decreased NF-κB activity. Different levels of NF-κB activation between the two *IKBKG* genotypes studied by us supported this finding. Both the *IKBKG*exon4_10 deletion and the less deleterious *IKBKG* missense variant, c.460C > T featured lower NF-κB activity compared controls. Thus, BM-MSCs of *IKBKG* mutation-positive women might have impaired NF-κB signalling in the bone marrow microenvironment.

Thus, the normal macroscopic bone phenotype we documented in clinically affected *IKBKG* mutation-positive women is unexplained. However, regulation of NF-κB is highly complex [44,45], and other pathways including the mitogen-activated protein kinase (MAPK) pathway [46], the phospholipase C-gamma (PLCγ) pathway [47], or Jun N-terminal kinase (JNK) signalling, which have opposite cellular effects compared to NF-κB [48], could theoretically compensate for decreased NF-κB activity in female *IKBKG* mutation carriers.

Furthermore, hemizygous mutation-positive males with IP carry only one hypomorphic *IKBKG* allele whereas the heterozygous females have cells containing both a mutated and a normal *IKBKG* allele. X-inactivation is the random and irreversible process of silencing either the paternally or maternally inherited X chromosome in individuals who carry two X-chromosomes. Typically, active and inactive X

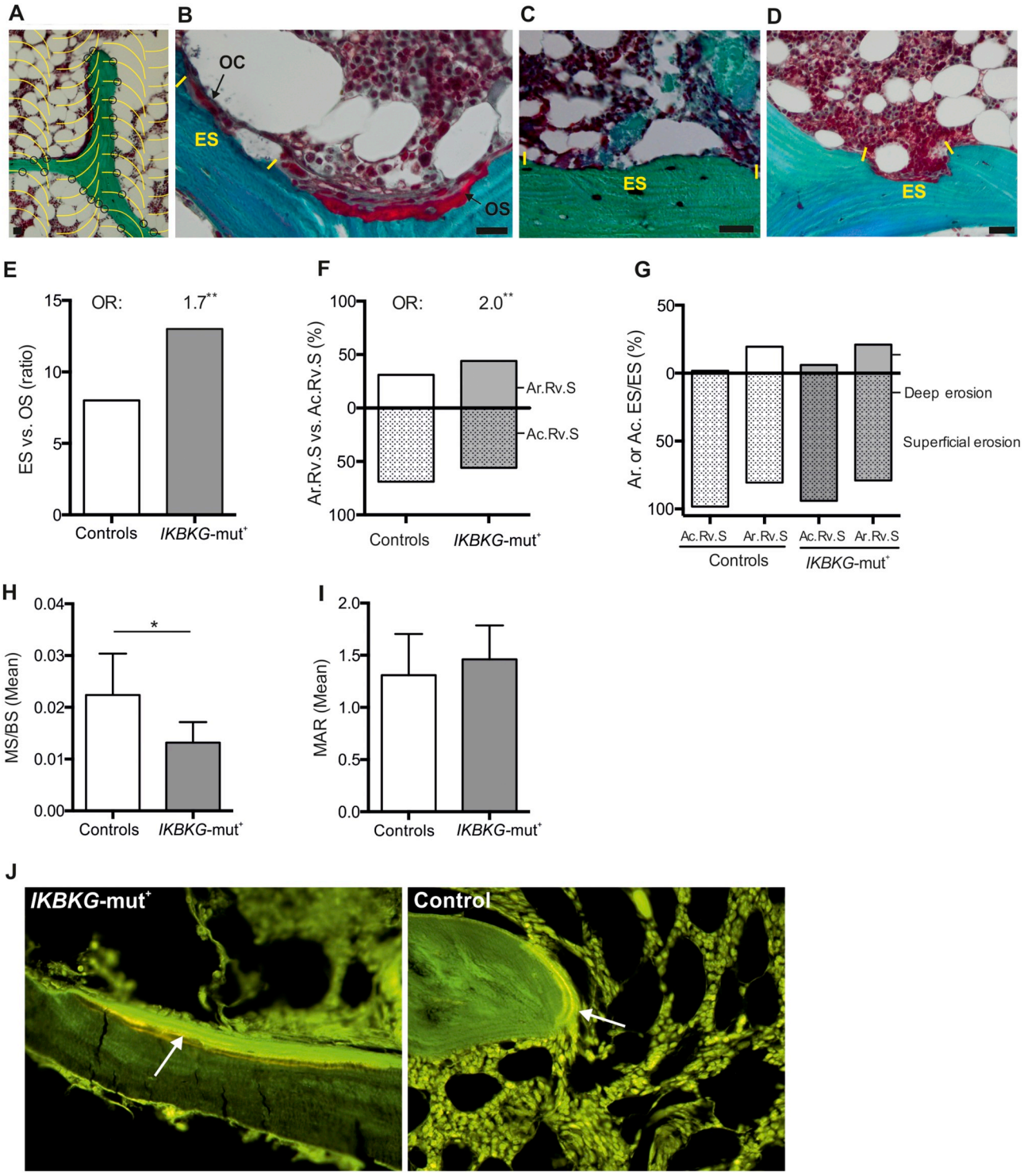

Fig. 2. Histology and histomorphometry of iliac crest bone in *IKBKG* mutation-positive carriers versus controls. Micrographs of Goldner's Trichrome stained sections printed as maps show eroded surface (ES), osteoid surface (OS), osteoclast surface (Oc.S), reversal surface (Rv.S), and quiescent surface (QS) marked on the bone surfaces. The prevalence's were calculated by intercepts (indicated by a black circle) between the particular surfaces and a cycloid grid (A). Histological appearance of an active eroded surface with OC and osteoid surfaces (B) and arrested Rv.Ss with no neighboring osteoid or Oc surfaces showing superficial erosion (C) and deep erosion (D). *IKBKG* mutation carriers show 1.7–fold higher extent of eroded surfaces relative to osteoid surfaces (E) and 2.0–fold higher proportion of arrested vs. active Rv.S (F). The arrested vs. active Rv.S have a 5.2–fold higher proportion of superficial resorption depths relative to deep erosion depths (G). MS/BS was significantly higher in controls vs. *IKBKG* mutation carriers (0.022 [0.019–0.029] vs. 0.013 [0.010–0.016], p = 0.03) (H), whereas no significant difference are found in mineral apposition rate (MAR) comparing *IKBKG* mutation carriers with controls (I). Fluorescent images of tetracycline double labeled iliac crest biopsy of an *IKBKG* mutation carrier and a control. The white arrows mark the tetracycline label (J).

Table 6
Static histomorphometric analysis in *IKBKG* mutation carrier versus controls.

	IKBKG mut$^+$ carriers	Controls	p-Value
QS/BS (%)	76.7 [54.2–89.8]	75.9 [69.3–80.8]	p = 0.62
ES/BS (%)	20.2 [9.7–42.4]	17.6 [15.0–21.6]	p = 0.99
OS/BS (%)	2.8 [0.4–6.2]	6.2 [0.7–14.1]	p = 0.09

Eroded surface (ES), osteoid surface (OS), quiescent surface (QS), and bone surface (BS). Median [range].

chromosomes are distributed around the mean of 50:50, but distributions > 80:20%, which is called "severely skewed X-inactivation" [49], is a phenomenon observed in ~10% of the healthy female population [50].

In 1996, Parrish et al. [15] reported that *IKBKG* mutation-positive women have severely skewed X-inactivation in peripheral blood leucocytes, with a possible selection against the mutated X-chromosome. Further, in a case-report from 2005, an age-associated negative selection against X-chromosomes with *IKBKG* mutations was demonstrated in the blood of a girl [51] and a boy with somatic mosaicism for a *IKBKG* stop mutation, c.937C > T (p.Gln313*) [52]. In our study, all seven *IKBKG* mutation carriers showed severely skewed X-inactivation in blood leucocytes, but not in BM-MSCs, and in case no. 6 the *IKBKG* mutated X was completely silenced. Thus, the combination of skewed X-inactivation and age-associated selection against bone cell-lines harbouring an active *IKBKG* mutated X-chromosome could explain how most bone cells in these *IKBKG* mutation-positive women have an active (i.e. non-mutated) *IKBKG* allele, containing sufficient NF-κB

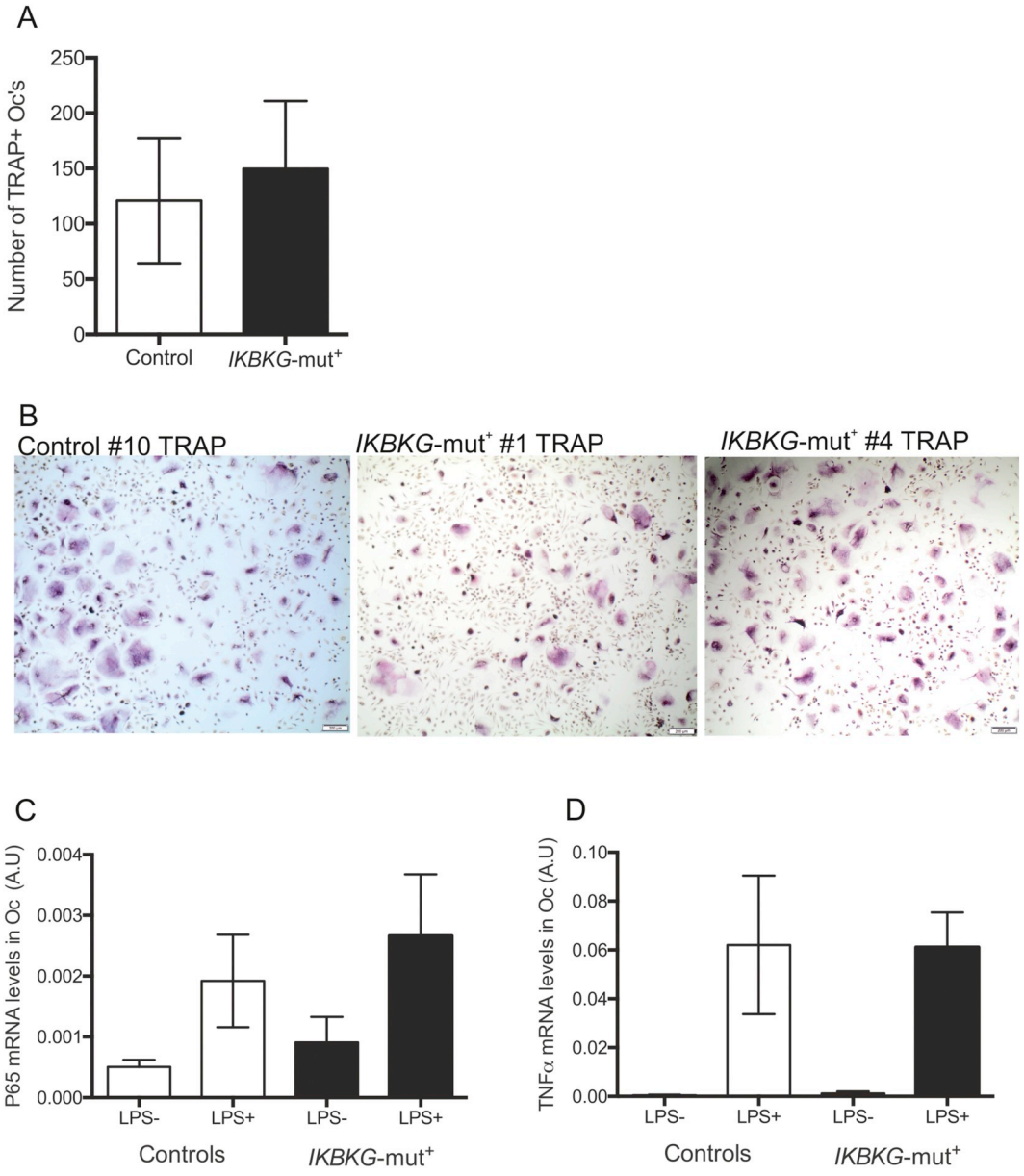

Fig. 3. (A) Number of TRAP-positive Ocs in *IKBKG* mutation carriers (n = 7) vs. controls (n = 7). Data are presented as mean ± SEM. No differences are found between *IKBKG* mut$^+$ carriers vs. controls (121 ± 57 vs. 150 ± 61, p = 0.75).
(B) Representative pictures of TRAP (purple) staining of Ocs in controls and *IKBKG* mut$^+$ carriers (scale bar 200 μm).
(C) mRNA levels (A.U.) of p65 (RelA) in Ocs before and after LPS stimulation. *IKBKG* mut$^+$ (n = 7) vs. controls (n = 7) (0.003 ± 0.001 vs. 0.002 ± 0.001, p = 0.59).
(D) mRNA levels of TNFα (A.U.) in Ocs before and after LPS. *IKBKG* mut$^+$ vs. controls (0.061 ± 0.014 vs. 0.062 ± 0.028, p = 0.98) Data are presented as mean ± SEM.

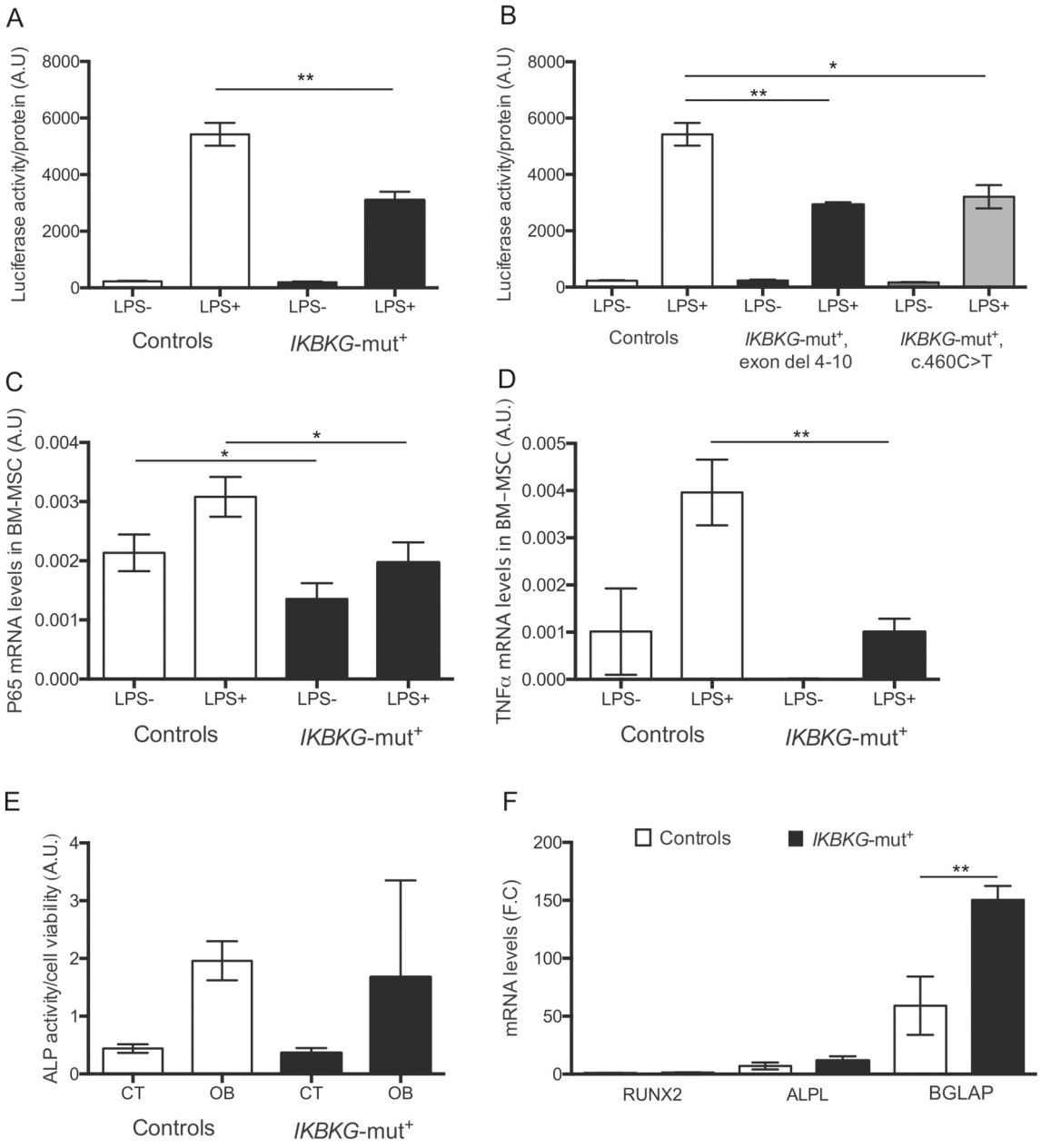

Fig. 4. (A) NF-κB activity expressed as luciferase activity normalized to protein concentration (A.U.) in BM-MSCs before and after LPS stimulation (LPS +). Controls (n = 5) vs. *IKBKG* mutation carrier (n = 5). Data are presented as mean ± SEM.
IKBKG mutation carriers have lower NF-κB activity in BM-MSCs compared to controls (3094 ± 679 vs. 5425 ± 899 μg protein, $p < 0.01$).
(B) NF-κB activity in BM-MSCs expressed as luciferase activity normalized to protein concentration (A.U.) before and after LPS stimulation (LPS +). Controls (n = 5) vs. *IKBKG*exon4_10del (n = 2) and *IKBKG*, c.460C > T (n = 3). Data are presented as mean ± SEM.
*IKBKG*exon4_10del and *IKBKG*, c.460C > T showing lower NF-κB activity in BM-MSCs compared to controls (2922 ± 93 and 3209 ± 412, vs. 5425 ± 402/μg protein, $p < 0.01$).
(C) mRNA levels of p65 (RelA) (A.U.) in BM-MSCs before and after LPS stimulation. Controls vs. *IKBKG* mutation carriers. Data are presented as mean ± SEM.
IKBKG mutation carriers showing lower gene expression of p65 (RELA) compared to controls (0.0031 ± 0.0008, vs. 0.0020 ± 0.0008 $p < 0.01$).
(D) mRNA levels of TNFα (A.U.) in BM-MSCs before and after LPS. Controls (n = 5) vs. *IKBKG* mutation carriers (n = 5). Data are presented as mean ± SEM.
IKBKG mutation carriers have lower gene expression of TNFα compared to controls (0.0039 ± 0.0020 vs. 0.0010 ± 0.0001, $p < 0.01$).
(E–F) Osteoblast differentiation potential of the BM-MSC evaluated by (E) quantification of ALP activity (day 10) (1.68 ± 0.76 vs. 1.96 ± 0.34, $p = 0.76$) and (F) gene expression of osteoblastic marker genes in *IKBKG* mutation carriers (n = 5) vs. controls (n = 5): (*RUNX2*: 1.33 ± 0.26 vs. 1.06 ± 0.09, $p = 0.34$; *ALPL*: 11.58 ± 3.81 vs. 7.04 ± 2.99, $p = 0.38$; *BGLAP*: 150.36 ± 12.08 vs. 59.03 ± 25.19, $p = 0.01$) represented as fold change (F.C.) over non-induced cells. Data are presented as mean ± SEM.

activity to account for their essentially normal skeletons. Circulating monocytes are precursors of Ocs, and X-inactivation may have occurred at this stage of Oc development [53]. We found normal Oc differentiation from PBMC in response to M-CSF and RANKL stimulation, and quantification of TRAP positive Ocs revealed no difference between *IKBKG* mutation carriers and controls, indicating that the skewed X-inactivation may partly account for the absence of an OPT bone phenotype in women.

*IKBKG*exon4_10del, the most common *IKBKG* mutation [17], is lethal to males in utero [18]. Thus, an apparent OPT phenotype has been

reported only in boys carrying less deleterious *IKBKG* mutations [19–21,23]. However, two additional genetic phenomena: i) somatic mosaicism and ii) 47,XXY karyotype (Klinefelter syndrome); i.e. males who carry an additional X chromosome, respectively, may enable these males to survive despite harbouring *IKBKG*exon4_10del. Subjects representing somatic mosaicism for an *IKBKG* mutation are comprised of a fraction of cells with wild-type as well as a fraction of cells with the mutated *IKBKG* gene, whereas subjects with Klinefelter syndrome and IP manifest skewed X-inactivation [54]. Although information from radiographic skeletal surveys is limited, abnormal bone phenotypes have not been reported in boys with somatic mosaicism for IP, or in boys with IP and Klinefelter syndrome, 47,XXY [55–57]. In particular, a 1-year-old boy with IP and 47,XXY, reportedly had normal radiographic findings [58]. These reports together with our findings suggest that individuals with two X-chromosomes (one harbouring an *IKBKG* mutation and the other a normal allele) will not have a OPT bone phenotype.

Our study has several limitations. Firstly, IP is rare; i.e. a birth prevalence of 1:40,000–140,000 [59,60], which hampers investigation of mutation-positive women. Therefore, our study population included relativ few subjects, yet this seems not to explain why we observed no significant abnormalities in the radiographs, DXA BMD, or biochemical bone turnover marker levels between *IKBKG* mutation carriers and controls.

Furthermore, the *IKBKG* mutation-positive females represented wide ranges in age and BMI, parameters with independent effects on BMD. With increasing age, bones become more fragile and change morphologically [61], and a positive association emerges between BMI and BMD [62,63]. Thus, this may have obscured effects from the two *IKBKG* mutations that we studied.

Finally, X-inactivation was highly skewed in our *IKBKG* mutation carriers, as previously reported for their patients by Migeon et al. [64] Determination of parental origin of the inactive X chromosome was, however, possible in only one of our patients (Table 1, case no. 6) who showed inactivation of the maternal; (i.e. the *IKBKG* mutated) X chromosome. For our other *IKBKG* mutation carriers, we could not determine if the normal X or the *IKBKG*-mutated X chromosome was silenced.

Nevertheless, the strength of our study is that it represents the largest assessment of bone characteristics, including bone morphology, microarchitecture, and bone remodeling, along with molecular analyses of BM-MSCs, in humans harbouring a mutation in *IKBKG*. In addition, ours is a case-control study of women harbouring two different *IKBKG* genotypes, including quantitation of X-inactivation in both blood leukocytes and BM-MSCs.

In conclusion, women with IP and carrying either of two specific *IKBKG* mutations demonstrated no signs of the OPT reported in affected hemizygous boys. Additional studies are necessary to better understand the pathogenesis of the minor histomorphometric bone changes in these women.

Funding sources

The study was supported by A.P. Moeller and Chastine Mc-Kinney Moeller Foundation for General Purposes, Region of Southern Denmark, Odense University Research Foundation, Aase og Ejnar Danielsens Fond, Novo Nordisk Foundation (NNF15OC0016284), and Shriners Hospitals for Children. MT was supported by a postdoctoral fellowship grant from the Danish Diabetes Academy supported by the Novo Nordisk Foundation. DJV and AZ were supported by NIH (AR070030).

Disclosures

The authors have no disclosures.

Acknowledgements

We thank Lotte Hørlyck, Birgit MacDonald, Kaja Søndergaard Laursen, Tina Kamilla Nielsen and Florence Figeac for excellent laboratory work.

We are grateful to Yousef Abu-Amer, Ph.D. for helpful review of our manuscript.

Study design: MF, MPW, ALF. Study conduct: ALF, CE, DS. Data collection: ALF, MT, CE, AZ, DJV. Data analysis: ALF, CMA, TLA, DJV, MPW. Data interpretation: MF, MT, CMA, TLA, DJV, MPW, ALF. Drafting manuscript: ALF. Revising manuscript content: MF, MPW and ALF. Approving final version of manuscript: All authors.

References

[1] A.S. Baldwin, The NF-kappa B and I kappa B proteins: new discoveries and insights, Annu. Rev. Immunol. 14 (1996) 649–683.
[2] J.C. Crockett, D.J. Mellis, D.I. Scott, M.H. Helfrich, New knowledge on critical osteoclast formation and activation pathways from study of rare genetic diseases of osteoclasts: focus on the RANK/RANKL axis, Osteoporos. Int. 22 (1) (Jan 2011) 1–20.
[3] D.V. Novack, Role of NF-κB in the skeleton, Cell Res. 21 (1) (Jan 2011) 169–182.
[4] G. Ghosh, G. van Duyne, S. Ghosh, P.B. Sigler, Structure of NF-kappa B p50 homodimer bound to a kappa B site, Nature 373 (6512) (Jan 1995) 303–310.
[5] V. Iotsova, J. Caamaño, J. Loy, Y. Yang, A. Lewin, R. Bravo, Osteopetrosis in mice lacking NF-kappaB1 and NF-kappaB2, Nat. Med. 3 (11) (Nov 1997) 1285–1289.
[6] W.C. Dougall, et al., RANK is essential for osteoclast and lymph node development, Genes Dev. 13 (18) (Sep 1999) 2412–2424.
[7] L. Gilbert, et al., Inhibition of osteoblast differentiation by tumor necrosis factor-alpha, Endocrinology 141 (11) (Nov 2000) 3956–3964.
[8] Y. Li, A. Li, K. Strait, H. Zhang, M.S. Nanes, M.N. Weitzmann, Endogenous TNFalpha lowers maximum peak bone mass and inhibits osteoblastic Smad activation through NF-kappaB, J. Bone Miner. Res. 22 (5) (May 2007) 646–655.
[9] N. Alles, et al., Suppression of NF-kappaB increases bone formation and ameliorates osteopenia in ovariectomized mice, Endocrinology 151 (10) (Oct 2010) 4626–4634.
[10] S. Hirata-Tsuchiya, et al., Inhibition of BMP2-induced bone formation by the p65 subunit of NF-κB via an interaction with Smad4, Mol. Endocrinol. 28 (9) (Sep 2014) 1460–1470.
[11] D. Rudolph, et al., Severe liver degeneration and lack of NF-kappaB activation in NEMO/IKKgamma-deficient mice, Genes Dev. 14 (7) (Apr 2000) 854–862.
[12] G. Swarnkar, et al., Myeloid deletion of nemo causes osteopetrosis in mice owing to upregulation of transcriptional repressors, Sci. Rep. 6 (2016) 29896.
[13] J. Chang, et al., Inhibition of osteoblastic bone formation by nuclear factor-kappaB, Nat. Med. 15 (6) (Jun 2009) 682–689.
[14] M.I. Conte, et al., Insight into IKBKG/NEMO locus: report of new mutations and complex genomic rearrangements leading to incontinentia pigmenti disease, Hum. Mutat. 35 (2) (Feb 2014) 165–177.
[15] J.E. Parrish, A.E. Scheuerle, R.A. Lewis, M.L. Levy, D.L. Nelson, Selection against mutant alleles in blood leukocytes is a consistent feature in Incontinentia Pigmenti type 2, Hum. Mol. Genet. 5 (11) (Nov 1996) 1777–1783.
[16] P.D. Stenson, M. Mort, E.V. Ball, K. Shaw, A. Phillips, D.N. Cooper, The Human Gene Mutation Database: building a comprehensive mutation repository for clinical and molecular genetics, diagnostic testing and personalized genomic medicine, Hum. Genet. 133 (1) (Jan 2014) 1–9.
[17] F. Fusco, et al., Incontinentia pigmenti: report on data from 2000 to 2013, Orphanet J. Rare Dis. 9 (2014) 93.
[18] F. Fusco, et al., Alterations of the IKBKG locus and diseases: an update and a report of 13 novel mutations, Hum. Mutat. 29 (5) (May 2008) 595–604.
[19] R. Döffinger, et al., X-linked anhidrotic ectodermal dysplasia with immunodeficiency is caused by impaired NF-kappaB signaling, Nat. Genet. 27 (3) (Mar 2001) 277–285.
[20] S. Mansour, et al., Incontinentia pigmenti in a surviving male is accompanied by hypohidrotic ectodermal dysplasia and recurrent infection, Am. J. Med. Genet. 99 (2) (Mar 2001) 172–177.
[21] C.M. Roberts, J.E. Angus, I.H. Leach, E.M. McDermott, D.A. Walker, J.C. Ravenscroft, A novel NEMO gene mutation causing osteopetrosis, lymphoedema, hypohidrotic ectodermal dysplasia and immunodeficiency (OL-HED-ID), Eur. J. Pediatr. 169 (11) (Nov 2010) 1403–1407.
[22] S. Ricci, F. Romano, F. Nieddu, C. Picard, C. Azzari, OL-EDA-ID syndrome: a novel hypomorphic NEMO mutation associated with a severe clinical presentation and transient HLH, J. Clin. Immunol. 37 (1) (Jan 2017) 7–11.
[23] S. Dupuis-Girod, et al., Osteopetrosis, lymphedema, anhidrotic ectodermal dysplasia, and immunodeficiency in a boy and incontinentia pigmenti in his mother, Pediatrics 109 (6) (Jun 2002) e97.
[24] K.H. Ørstavik, et al., Novel splicing mutation in the NEMO (IKK-gamma) gene with severe immunodeficiency and heterogeneity of X-chromosome inactivation, Am. J. Med. Genet. A 140 (1) (Jan 2006) 31–39.
[25] N. Guañabens, et al., Idiopathic acquired osteosclerosis in a middle-aged woman with systemic lupus erythematosus, J. Bone Miner. Res. 31 (9) (September 2016) 1774–1782.
[26] R.C. Allen, H.Y. Zoghbi, A.B. Moseley, H.M. Rosenblatt, J.W. Belmont, Methylation

of HpaII and HhaI sites near the polymorphic CAG repeat in the human androgen-receptor gene correlates with X chromosome inactivation, Am. J. Hum. Genet. 51 (6) (Dec 1992) 1229–1239.
[27] J. Hanson, Standardization of femur BMD, J. Bone Miner. Res. 12 (8) (Aug 1997) 1316–1317.
[28] R.R. Recker, M.P. Akhter, J.M. Lappe, P. Watson, Bone histomorphometry in transiliac biopsies from 48 normal, healthy men, Bone 111 (Jun 2018) 109–115.
[29] M. Ding, A. Odgaard, F. Linde, I. Hvid, Age-related variations in the microstructure of human tibial cancellous bone, J. Orthop. Res. 20 (3) (May 2002) 615–621.
[30] T. Hildebrand, P. Rüegsegger, Quantification of bone microarchitecture with the structure model index, Comput. Methods Biomech. Biomed. Engin. 1 (1) (1997) 15–23.
[31] C.M. Andreasen, M. Ding, S. Overgaard, P. Bollen, T.L. Andersen, A reversal phase arrest uncoupling the bone formation and resorption contributes to the bone loss in glucocorticoid treated ovariectomised aged sheep, Bone 75 (Jun 2015) 32–39.
[32] T.L. Andersen, et al., Understanding coupling between bone resorption and formation: are reversal cells the missing link? Am. J. Pathol. 183 (1) (Jul 2013) 235–246.
[33] D.W. Dempster, et al., Standardized nomenclature, symbols, and units for bone histomorphometry: a 2012 update of the report of the ASBMR Histomorphometry Nomenclature Committee, J. Bone Miner. Res. 28 (1) (Jan 2013) 2–17.
[34] P. Boissy, T.L. Andersen, B.M. Abdallah, M. Kassem, T. Plesner, J.M. Delaissé, Resveratrol inhibits myeloma cell growth, prevents osteoclast formation, and promotes osteoblast differentiation, Cancer Res. 65 (21) (Nov 2005) 9943–9952.
[35] B.M. Abdallah, M. Haack-Sorensen, T. Fink, M. Kassem, Inhibition of osteoblast differentiation but not adipocyte differentiation of mesenchymal stem cells by sera obtained from aged females, Bone 39 (1) (Jul 2006) 181–188.
[36] I. Alam, et al., Phenotypic severity of autosomal dominant osteopetrosis type II (ADO2) mice on different genetic backgrounds recapitulates the features of human disease, Bone 94 (January 2017) 34–41.
[37] J.W. Milgram, M. Jasty, Osteopetrosis. A morphological study of twenty-one cases, J. Bone Joint Surg. Am. 64 (6) (Jul 1982) 912–929.
[38] M.M. Guerrini, et al., Human osteoclast-poor osteopetrosis with hypogammaglobulinemia due to TNFRSF11A (RANK) mutations, Am. J. Hum. Genet. 83 (1) (Jul 2008) 64–76.
[39] R. Baron, Importance of the intermediate phases between resorption and formation in measurement and understanding of the bone remodeling sequence, in: P.J. Meaner (Ed.), Bone Histomorphometry: Second International Workshop Lyon, Armour Mantagu, Toulouse, 1977, pp. 179–183.
[40] R.S. Weinstein, Glucocorticoid-induced osteoporosis, Rev. Endocr. Metab. Disord. 2 (1) (Jan 2001) 65–73.
[41] P.R. Jensen, T.L. Andersen, E.M. Hauge, J. Bollerslev, J.M. Delaissé, A joined role of canopy and reversal cells in bone remodeling—lessons from glucocorticoid-induced osteoporosis, Bone 73 (Apr 2015) 16–23.
[42] P.R. Jensen, T.L. Andersen, B.L. Pennypacker, L.T. Duong, L.H. Engelholm, J.M. Delaissé, A supra-cellular model for coupling of bone resorption to formation during remodeling: lessons from two bone resorption inhibitors affecting bone formation differently, Biochem. Biophys. Res. Commun. 443 (2) (Jan 2014) 694–699.
[43] N.E. Lassen, et al., Coupling of bone resorption and formation in real time: new knowledge gained from human Haversian BMUs, J. Bone Miner. Res. 32 (7) (Jul 2017) 1395–1405.
[44] N.D. Perkins, Integrating cell-signalling pathways with NF-kappaB and IKK function, Nat. Rev. Mol. Cell Biol. 8 (1) (Jan 2007) 49–62.
[45] G. Ghosh, V.Y. Wang, D.B. Huang, A. Fusco, NF-κB regulation: lessons from structures, Immunol. Rev. 246 (1) (Mar 2012) 36–58.
[46] A. Gingery, E. Bradley, A. Shaw, M.J. Oursler, Phosphatidylinositol 3-kinase coordinately activates the MEK/ERK and AKT/NFkappaB pathways to maintain osteoclast survival, J. Cell. Biochem. 89 (1) (May 2003) 165–179.
[47] D. Mao, H. Epple, B. Uthgenannt, D.V. Novack, R. Faccio, PLCgamma2 regulates osteoclastogenesis via its interaction with ITAM proteins and GAB2, J. Clin. Invest. 116 (11) (Nov 2006) 2869–2879.
[48] J.L. Luo, H. Kamata, M. Karin, IKK/NF-kappaB signaling: balancing life and death—a new approach to cancer therapy, J. Clin. Invest. 115 (10) (Oct 2005) 2625–2632.
[49] F. Fusco, et al., Molecular analysis of the genetic defect in a large cohort of IP patients and identification of novel NEMO mutations interfering with NF-kappaB activation, Hum. Mol. Genet. 13 (16) (Aug 2004) 1763–1773.
[50] A. Sharp, D. Robinson, P. Jacobs, Age- and tissue-specific variation of X chromosome inactivation ratios in normal women, Hum. Genet. 107 (4) (Oct 2000) 343–349.
[51] N. Martinez-Pomar, I. Munoz-Saa, D. Heine-Suner, A. Martin, A. Smahi, N. Matamoros, A new mutation in exon 7 of NEMO gene: late skewed X-chromosome inactivation in an incontinentia pigmenti female patient with immunodeficiency, Hum. Genet. 118 (3–4) (Dec 2005) 458–465.
[52] S. Hull, et al., Somatic mosaicism of a novel IKBKG mutation in a male patient with incontinentia pigmenti, Am. J. Med. Genet. A 167 (7) (Jul 2015) 1601–1604.
[53] M. Geens, S.M. Chuva De Sousa Lopes, X chromosome inactivation in human pluripotent stem cells as a model for human development: back to the drawing board? Hum. Reprod. Update 23 (5) (Sep 2017) 520–532.
[54] S. Kenwrick, et al., Survival of male patients with incontinentia pigmenti carrying a lethal mutation can be explained by somatic mosaicism or Klinefelter syndrome, Am. J. Hum. Genet. 69 (6) (Dec 2001) 1210–1217.
[55] E. Buinauskaite, J. Buinauskiene, V. Kucinskiene, D. Strazdiene, S. Valiukeviciene, Incontinentia pigmenti in a male infant with Klinefelter syndrome: a case report and review of the literature, Pediatr. Dermatol. 27 (5) (Sep–Oct 2010) 492–495.
[56] J. García-Dorado, P. de Unamuno, E. Fernández-López, J. Salazar Veloz, M. Armijo, Incontinentia pigmenti: XXY male with a family history, Clin. Genet. 38 (2) (Aug 1990) 128–138.
[57] L.M. Franco, et al., Incontinentia pigmenti in a boy with XXY mosaicism detected by fluorescence in situ hybridization, J. Am. Acad. Dermatol. 55 (1) (Jul 2006) 136–138.
[58] J.S. Prendiville, J.L. Gorski, C.K. Stein, N.B. Esterly, Incontinentia pigmenti in a male infant with Klinefelter syndrome, J. Am. Acad. Dermatol. 20 (5 Pt 2) (May 1989) 937–940.
[59] C.C. Swinney, D.P. Han, P.A. Karth, Incontinentia pigmenti: a comprehensive review and update, Ophthalmic. Surg. Lasers Imaging Retina 46 (6) (Jun 2015) 650–657.
[60] R.G. Carney, Incontinentia pigmenti. A world statistical analysis, Arch. Dermatol. 112 (4) (Apr 1976) 535–542.
[61] S.M. Tommasini, P. Nasser, K.J. Jepsen, Sexual dimorphism affects tibia size and shape but not tissue-level mechanical properties, Bone 40 (2) (Feb 2007) 498–505.
[62] D.T. Felson, Y. Zhang, M.T. Hannan, J.J. Anderson, Effects of weight and body mass index on bone mineral density in men and women: the Framingham study, J. Bone Miner. Res. 8 (5) (May 1993) 567–573.
[63] I.R. Reid, Fat and bone, Arch. Biochem. Biophys. 503 (1) (Nov 2010) 20–27.
[64] B.R. Migeon, J. Axelman, S. Jan de Beur, D. Valle, G.A. Mitchell, K.N. Rosenbaum, Selection against lethal alleles in females heterozygous for incontinentia pigmenti, Am. J. Hum. Genet. 44 (1) (Jan 1989) 100–106.